ACS APPLIED MATERIALS & INTERFACES

Research Article

www.acsami.org

Purification of Nanoscale Electron-Beam-Induced Platinum Deposits via a Pulsed Laser-Induced Oxidation Reaction

Michael G. Stanford,[†] Brett B. Lewis,[†] Joo Hyon Noh,[†] Jason D. Fowlkes,[‡] Nicholas A. Roberts,[§] Harald Plank,[∥] and Philip D. Rack*[,†,‡]

[†]Materials Science and Engineering Department, University of Tennessee, Knoxville, Tennessee 37996, United States

[‡]Nanofabrication Research Laboratory, Center for Nanophase Materials Sciences, Oak Ridge National Laboratory, Oak Ridge, Tennessee 37381, United States

[§]Department of Mechanical and Aerospace Engineering, Utah State University, Logan, Utah 84322, United States

[∥]Institute for Electron Microscopy and Nanoanalysis, Graz University of Technology, Steyrergasse 17, 8010 Graz, Austria

Supporting Information

ABSTRACT: Platinum−carbon deposits made via electron-beam-induced deposition were purified via a pulsed laser-induced oxidation reaction and erosion of the amorphous carbon to form pure platinum. Purification proceeds from the top down and is likely catalytically facilitated via the evolving platinum layer. Thermal simulations suggest a temperature threshold of ∼485 K, and the purification rate is a function of the PtC_5 thickness (80−360 nm) and laser pulse width (1−100 μs) in the ranges studied. The thickness dependence is attributed to the ∼235 nm penetration depth of the PtC_5 composite at the laser wavelength, and the pulse-width dependence is attributed to the increased temperatures achieved at longer pulse widths. Remarkably fast purification is realized at cumulative laser exposure times of less than 1 s.

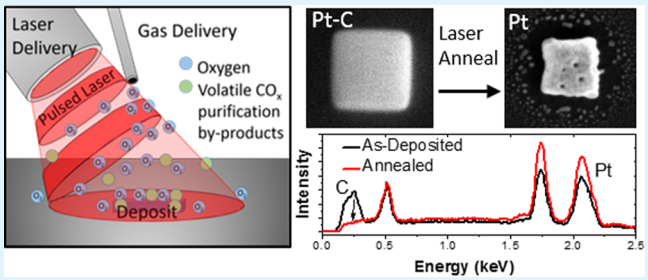

KEYWORDS: *focused electron-beam-induced deposition, platinum, pulsed laser, annealing, nanofabrication, purification*

INTRODUCTION

Electron-beam-induced deposition (EBID) is a synthesis technique that is dictated by a focused electron beam and stimulates a localized reaction of precursor species.[1−3] The result is a nanoscale synthesis technique that can conveniently grow materials "on-demand" via a prescribed electron-beam raster sequence. Significant advances have been made by elucidating the critical electron−precursor−solid interactions[4−8] that occur in the EBID process, which has enabled better control and higher resolution. Thus, several applications have emerged for nanostructured materials grown via EBID, such as specialized scanning probe tips,[9,10] nanomagnetic logic and devices,[11,12] nanophotonics,[13,14] field-emission emitters,[15,16] new sensor concepts exploiting nanogranular behavior,[17,18] maskless lithography,[19−22] lithography mask editing,[23−26] superconducting nanostructures,[27,28] and electrical contacts on-demand[29] to name a few.

While the field has experienced significant growth over the past decade, one of the main liabilities of focused electron (and ion)-beam-induced processing has been the inclusion of unwanted byproducts in the deposits. Byproduct inclusion occurs because EBID is typically performed at room temperature and the standard chemical vapor deposition (CVD) precursors utilized do not volatilize completely under the electron beam. For instance, one of the most common precursors used is the trimethyl(methylcyclopentadienyl)-platinum(IV) ($MeCpPt^{IV}Me_3$) precursor, which, depending on the electron-beam parameters used, deposits PtC_x material where $5 \leq x \leq 8$.[30,31] To address this limitation, several groups around the world have explored in situ and ex situ methods to purify EBID materials (see Botman et al.[1] for a review). While not an exhaustive list, some approaches that have been used include postsynthesis annealing,[32−34] more volatile precursors,[35−37] mixing of reactive gases to stimulate byproduct desorption,[38−40] in situ substrate heating with reactive gases,[41,42] and postelectron irradiation with[43,44] and without reactive gases.[45,46]

Selective optical coupling of EBID deposits could enable photothermal purification to be achieved with minimal damage to the surrounding features or substrates. For instance, we have investigated an in situ synchronized pulsed laser-assisted EBID (LAEBID) process in which an intermittent pulsed laser was used to thermally assist the desorption of carbonaceous byproducts from the $MeCpPt^{IV}Me_3$[47] and $W(CO)_6$[48] precursors during growth. To add to our understanding of conditions that affect the LAEBID process, here we investigate a postgrowth laser annealing process. Although similar to many of the postheating studies that have been performed, optical

Received: September 12, 2014
Accepted: November 5, 2014
Published: November 5, 2014

 © 2014 American Chemical Society

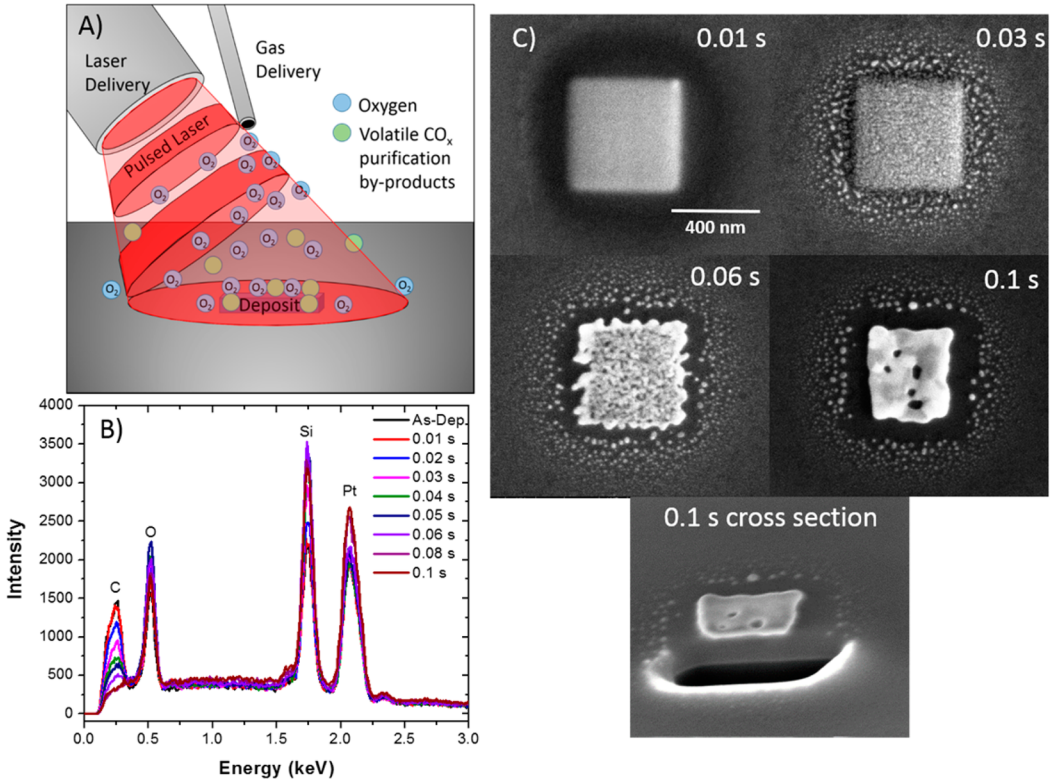

Figure 1. (A) Schematic of the laser annealing setup with approximately 100 μm laser spot size under O_2 flow. (B) EDS measurements of a ~140-nm-thick PtC_5 EBID deposit annealed with 100 μs pulses at 0.1% duty cycle as a function of the exposure times. (C) Images of laser-annealed patterns at different exposure times. The deposit annealed for 0.1 s exposure time was also cross-sectioned and is pictured here.

coupling can be tuned to be minimally invasive to the substrate or devices because of small laser spot size and precise control of pulsing conditions, which as we will show lead to a relatively short cumulative heating time.

In this study, we used an IR laser delivery system integrated onto our dual electron–ion beam system[48] to irradiate PtC_x (where x = 5) deposits in the presence of a localized O_2 flow from a gas-injection system (Figure 1A; see methods for details). As we will show, laser irradiation couples with the PtC_5 matrix and photothermally heats the deposit and stimulates a reaction of carbon with the localized flux of O_2 molecules. In contrast to our in situ synchronized process demonstrated previously,[47] no observable purification was accomplished without O_2 flow for the ex situ laser annealing process (see the Supporting Information, SI).

EXPERIMENTAL SECTION

EBID was performed in an FEI Nova Nanolab 600 DualBeam system (FEI Company; Hillsboro, OR). Silicon substrates with thermally grown 100 nm SiO_2 were plasma-cleaned (Evactron; XEI Scientific, Inc., Redwood City, CA) in the chamber for a minimum of 30 min prior to deposition. All PtC_5 EBID structures in this study were grown with the $MeCpPt^{IV}Me_3$ precursor at a chamber pressure of ~1.2 × 10^{-5} mbar and the gas nozzle ~100 μm above the substrate. EBID pads were grown to varible thicknesses by changing the number of electron passes or loops (1000, 2000, 4000, and 8000 loops) in a 500 × 500 nm^2 square pattern. The corresponding heights of these deposits are approximately 80, 140, 260, and 360 nm, respectively. Each pad pattern was deposited at 5 keV energy, 98 pA current, 10 μs dwell time, and 13.55 nm pixel pitch (50% overlap). Subsequent to deposition, the chamber was pumped for at least 30 min prior to laser annealing to minimize residual $MeCpPt^{IV}Me_3$ precursor in the chamber.

A 915-nm-wavelength 25 W multichip diode laser module (BMU25B-915-01; Oclaro Inc., San Jose, CA) driven by an IXYS PCX-7410 pulsed diode laser driver was used to anneal the EBID deposits. The laser delivery system (Omniprobe, Inc., Oxford, U.K.) was mounted ~38° relative to the substrate normal and precisely delivers a beam size of ~100 μm diameter, as schematically shown in Figure 1A. During laser irradiation, O_2 gas was delivered to the area of interest with an OmniGIS I (Oxford Instruments, Oxford, U.K.) gas injection system, which was positioned 100 μm above the substrate and 200 μm from the center of the field of view. The gas temperature was set to 25 °C, and the valve pulse rate was set such that the chamber pressure was 1.2 × 10^{-5} mbar. Because of the GIS needle position and the 100 μm laser spot size, large deposits within the entire laser spot can be annealed in a parallel manner. If larger areas need to be purified, we envision that sequential stage motions could be implemented to raster the area of interest under the focused laser with an appropriate beam overlap strategy employed. During this study, variable laser pulse widths (1, 10, and 100 μs) and duty cycles (0.1% and 1%) were used at a constant optical power density of ~165 kW/cm^2. Pulse-width and duty-cycle combinations were selected in such a way as to provide adequate cooling time between pulses for the substrate to return to room temperature. Obviously, the specific laser conditions are a function of the deposit and substrate, and thus different substrates will have different optimum conditions; thus, understanding both the laser absorption and subsequent thermal diffusion is critical, and for extremely delicate substrates, for instance membranes, thermal stresses need to be considered (see ref 47 for instance). More information on the laser delivery system can be found in ref 49.

Energy-dispersive X-ray spectroscopy (EDS) was performed with an EDAX Genesis X-ray Microanalysis System also mounted on the dual-beam system; thus, the samples were not exposed to the atmosphere. Each spectrum was recorded with beam conditions of 5 kV and 1.6 nA and a 30 s acquisition time. A 100 nm SiO_2-coated silicon substrate

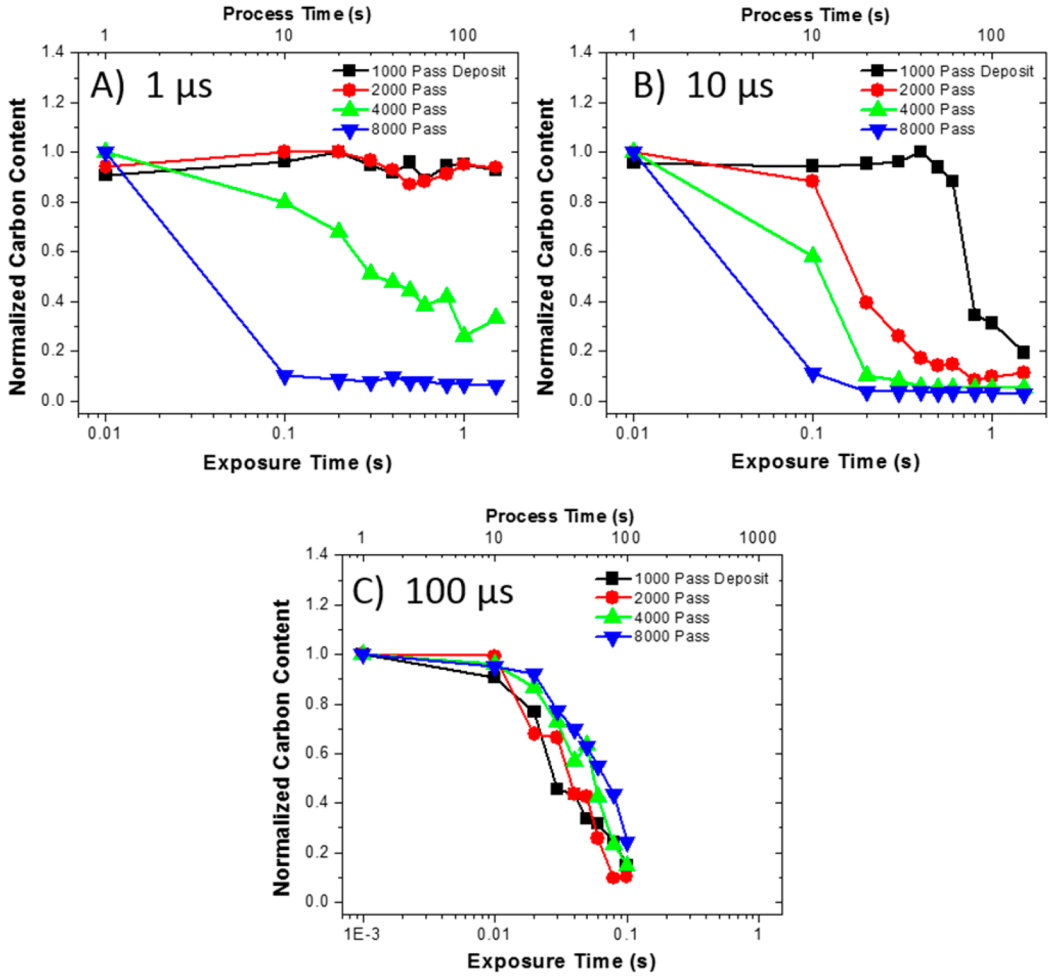

Figure 2. Carbon content as a function of the exposure time (duty cycle × processing time, bottom axis) and processing time (top axis) for (A) 1 μs at 1% duty cycle, (B) 10 μs at 1% duty cycle, and (C) 100 μs at 0.1% duty cycle. The initial pad thicknesses were ~80, 140, 260, and 350 nm.

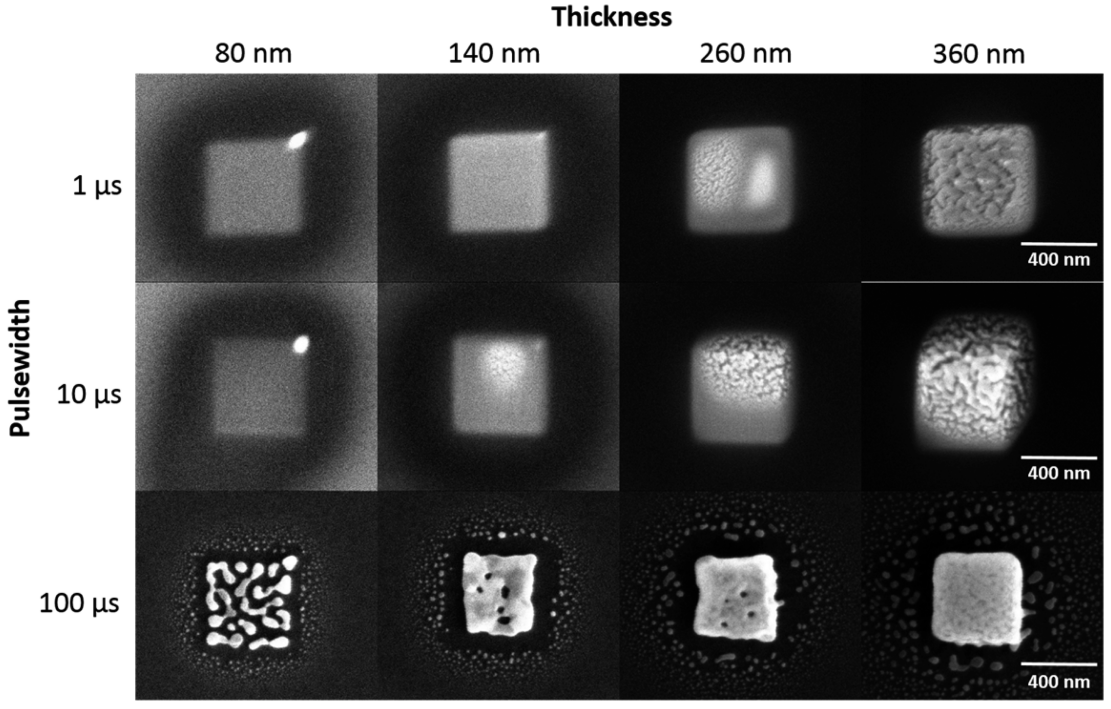

Figure 3. SEM images of PtC_5 deposits of variable thicknesses and annealing pulse widths that were annealed for 0.1 s of laser exposure time.

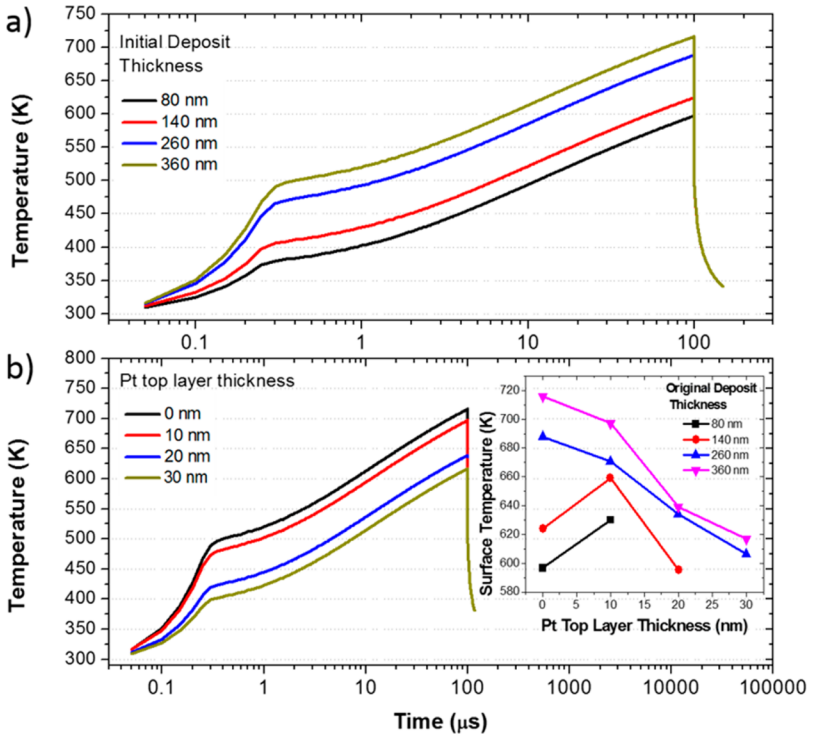

Figure 4. (a) Time−temperature thermal profile for deposits of variable thickness (inset) irradiated with a 100 μs laser pulse. (b) Simulated thermal profiles of the deposit surface as a function of the pure platinum top layer thickness (which represents purification) for a deposit that was initially 360 nm *prior* to annealing. Inset: maximum temperature at the deposit surface as a function of the platinum top layer thickness and original deposit thickness.

EDS scan was used to determine the background for data analysis and peak fitting (see the SI for an EDS analysis description).

RESULTS AND DISCUSSION

Figure 1B illustrates EDS measurements of a ∼140-nm-thick, 500 × 500 nm^2 square pattern of PtC_5 that was progressively laser-irradiated with 100 μs pulse width, 0.1% duty cycle, and ∼165 W/cm^2 optical power density under O_2 flux. Note that the laser exposure time (the product of the processing time and duty cycle) is 0.1% of the actual processing time. Clearly, the carbon peak (0.277 keV) in the 5 keV beam interaction region rapidly decreases with time and suggests purification from the PtC_5 deposit to pure platinum (within the detection limits of EDS). A small shoulder remains in this energy range, but as described previously by ref 43, the small residual peak can be attributed to the Pt−N peak. Images of progressive purification are presented in Figure 1C. The onset of platinum grain coarsening occurs rapidly (<0.3 s laser exposure time) as the carbon is reduced and continues until carbon removal is complete at approximately 1.0 s. Peripheral nanoparticles appear around the edges of the deposits once exposed to laser annealing. These particles are a result of peripheral deposition during the EBID process and can be minimized by the careful selection of electron-beam parameters during deposition.[50,51]

Subsequent to the initial laser series, three laser conditions (1 and 10 μs at 1% duty cycle and 100 μs at 0.1% duty cycle) were used to simultaneously anneal 500 × 500 nm^2 PtC_5 EBID deposits of variable thicknesses (∼80, 140, 260, and 360 nm). Figure 2A illustrates the integrated and normalized carbon EDS peak of the PtC_5 deposits as a function of the effective laser exposure time for 1 μs 1% duty cycle pulses (see the SI for EDS spectra and estimated purification rates). A higher duty cycle was used for the lower pulse width to accelerate purification. Interestingly, the thick deposits (260 and 360 nm) were rapidly purified, whereas the thin deposits (80 and 140 nm) were unaffected by this laser treatment. Figure 2B illustrates that the 10 μs 1% laser treatment purifies PtC_5 faster; however, thinner deposits again cure at slower rates than the thicker deposits. For deposits laser-treated with 100 μs 0.1% duty cycle conditions (Figure 2C), the annealing rate was effectively independent of the initial deposit height and very quick in comparison with 1 and 10 μs pulses.

We entertained the possibility of both pyrolytic and photolytic mechanisms for purification of PtC_5. Figure 3 compares the scanning electron microscopy (SEM) micrographs, normalized to a constant laser exposure time, which demonstrate purification progression as a function of the deposit thickness and laser pulse width. All deposits shown were subjected to an exposure time of 0.1 s. As illustrated in Figure 2, the thicker samples are purified at a higher rate than the thinner samples for 1 and 10 μs pulse widths, whereas the deposits irradiated with 100 μs pulses are all effectively annealed. Hence, the increase in the purification rate using 100 μs pulses is attributed to the thermal profile of the laser pulse, which reaches a higher temperature than the 1 and 10 μs pulses. We conclude that photolytic purification mechanisms are not dominant, as indicated by the differences in purification with variable pulse widths at a constant exposure time. Complementary EBID lines with variable thicknesses also clearly illustrate the thickness/laser-pulse-width dependence on purification (see the SEM images in the SI).

In order gain a better understanding of the laser annealing behavior, we estimated the optical and thermal properties of PtC_5 via a simple Maxwell−Garnett model of a platinum and

amorphous carbon composite. The refractive index (n) and extinction coefficient (κ) for the PtC_5 material were estimated to be 1.88 and 0.31, respectively; thus, the optical penetration depth $[(4\pi\kappa/\lambda)^{-1}]$ was estimated to be ~235 nm for PtC_5 deposits. Details of the methods used for estimating the relevant PtC_x material properties and a description of the subsequent finite-difference numerical approximation method used to perform the thermal simulations may be found in the SI. Figure 4a illustrates simulated temperature profiles as a function of the laser pulse width and different PtC_5 thicknesses. Clearly, the pulse-width temperatures do not reach steady state in the experimental pulse-width range as the temperature for each thickness rises over the entire range studied. Because of the PtC_5 penetration depth and low thermal conductivity, the thicker deposits are photothermally heated to higher temperatures relative to the optically thin deposits. Also, optically transparent SiO_2 is a good thermal insulator and minimizes silicide formation relative to silicon. These factors explain the faster annealing of the thicker deposits at short pulse widths.

We attribute photothermal purification of the PtC_5 deposits to a basic reaction of the carbon matrix with the localized O_2 flux. Thus, the process depends on both the temperature and oxygen concentration at the reaction front. Clearly, a threshold temperature must be reached in order to drive the reaction and erosion of the carbonaceous matrix. This is evident because the laser annealing processes, which result in lower simulated temperature per pulse (i.e., thin deposits at short pulse widths), do not effectively remove the carbon, despite having the same exposure time. Thermal chemical erosion of amorphous hydrogenated carbon has been shown to have a threshold of approximately 650 K.[52] Furthermore, high-purity platinum films via CVD using the $MeCpPt^{IV}Me_3$ precursor can be grown as low as 475 K; however, an interesting enhanced growth mode is observed at ~550 K, which is driven by an autocatalytic oxidation decomposition reaction.[53] Comparing the thermal simulations with our observable purification of PtC_5 reveals an erosion threshold of approximately 485 K for carbon in the PtC_5 deposits. The difference in the threshold temperature could be due to underestimating κ and/or overestimating n in our effective medium approximation because there are different literature values in particular for amorphous carbon. Additionally, and consistent with the autocatalytic CVD process, purification may be facilitated by catalytic O_2–Pt reactions, whereby O_2 dissociatively adsorbs to create atomic oxygen, which is much more reactive and could lower the reaction temperature.[53−55] The catalytic contribution will be considered more thoroughly in a future model description of the process, but recently it has been suggested in a thermally activated PtC_x purification process in which an O_2 flux is periodically pulsed.[56] Qualitatively, the results indicate that the O_2–C does not effectively react in thin deposits at a 1 μs pulse width, whereas 10 and 100 μs laser pulse widths can effectively induce carbonaceous erosion in all of the deposit thicknesses tested here because each exceeds the temperature threshold.

Figure 5a contains SEM cross sections of laser-treated ~360-nm-thick PtC_5 deposits at different laser exposure times (10 μs 1% duty cycle), which illustrates the increase in the platinum layer thickness from the top down (see the SI for complementary images of the other laser conditions). Asymmetric purification (left face favored purification), observed in Figure 5a, is attributed to the geometry of the gas injection and laser delivery because both are delivered from the left side of the SEM image. Figure 5b plots the resultant

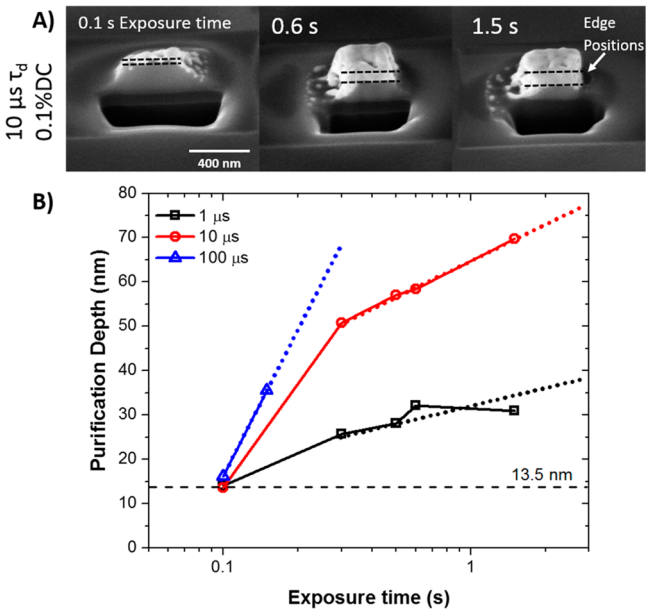

Figure 5. (A) Cross-sectional SEM images (at 52°) of a 360-nm-thick PtC_5 deposit annealed at 10 μs pulse width and 1.0% duty cycle conditions at variable exposure times (exposure times and superimposed edge positions are inset in the images). (B) Purification depth as a function of the exposure time for 1, 10, and 100 μs pulse-width laser conditions with a superimposed penetration depth of pure platinum (dotted line).

platinum thickness versus the laser exposure time for each laser treatment. The estimates show that, for the thick deposit, each laser condition converges toward the same thickness at 0.1 s exposure time, although this is difficult to conclusively measure because of the topology that develops. This is consistent with the fact that each condition exceeds the activation temperature, and while higher temperatures can accelerate the reaction rate, the O_2 flux eventually limits the extent of the reaction. Interestingly, beyond ~10 nm, the apparent growth rates diverge, which we will address below.

Mechanistically, the picture that emerges is that each laser pulse rapidly heats the deposit, which thermally stimulates the reaction of the amorphous carbon matrix with the O_2 flux and forms CO_x volatile byproducts. Reduction of carbon in the PtC_5 deposits causes an anticipated ~70% volume reduction, which is evident in Figures 1C and 5A.[43] Because of the relatively high concentration of O_2 impinging on the surface, an outer shell of pure platinum initially forms. After formation of the outer platinum shell, O_2 must permeate through platinum grains and the nanoscale porosity develops in order to sustain the purification process in the deposit interior. As the pure platinum layer nucleates and grows, the optical coupling changes because of the optical and thermal properties of pure platinum. Figure 4b shows simulated surface time–temperature profiles of progressively thicker platinum layers with concomitant 70% reduction in the PtC_5 layer due to carbon loss for a deposit with a 360 nm initial thickness (the surface time–temperature profiles for other thicknesses studied in this work are reported in the SI). The inset illustrates the simulated temperature as a function of the platinum layer thickness for the different original PtC_5 thicknesses. An interesting interplay occurs as the platinum layer grows, which varies for the different original PtC_5 thicknesses. For the two optically thick PtC_5 deposits, the growing platinum layer decreases the

dx.doi.org/10.1021/am506246z | ACS Appl. Mater. Interfaces 2014, 6, 21256−21263

temperature over the entire platinum thickness range; however, the surface temperature fluctuates. At 10 nm, the slight initial decrease is due to the high platinum reflectivity, which is partially compensated for by the high absorption because the film thickness is close to the penetration depth of 915 nm radiation. As the platinum layer increases beyond the penetration depth, the temperature further decreases because of the thermal mass of the additional platinum layer. We suggest that the reduced growth rate beyond 10 nm for the 360-nm-thick deposit noted in Figure 5B is due to the temperature difference at 1, 10, and 100 μs for the thicker platinum layers.

For the optically thin layers, as the thickness approaches the platinum penetration depth (~10 nm), there is positive feedback and the temperature supersedes the original surface temperature because of a significant increase in the absorbance of the deposit. As the platinum layer increases beyond the penetration depth, the temperature decreases similar to the thicker deposits because of the increased thermal mass.

To further illustrate the importance of optical coupling, we also deposited 80 nm PtC_5 layers on top of thin platinum layers (5, 10, and 20 nm) and irradiated the bilayers with conditions (10 μs and 1% duty cycle) that otherwise do not purify the optically thin PtC_5 layers (see the SI). As expected, the purification rate scaled with the platinum thickness because the enhanced optical coupling and reflectance associated with the pure platinum underlayer increase the temperature in the PtC_5 layer, which induces the combustion reaction of O_2 with the carbon matrix. Importantly, in this case, the PtC_5/Pt layer sequence reduces the reflectance and thus increases the overall temperature during the early stages of purification.

CONCLUSIONS AND OUTLOOK

In summary, we have demonstrated a new pseudo in situ technique to purify the EBID of PtC_5 deposits from the $MeCpPt^{IV}Me_3$ precursor. At the 165 kW/cm^2 power density studied here, the temperature increases with the laser pulse width. Furthermore, the composite PtC_5 material has an estimated absorption depth of 235 nm; thus, the temperature is also sensitive to the deposit thickness. A threshold temperature of ~485 K was estimated via simulations, which is lower than that previously determined for amorphous carbon combustion with O_2. Either the reduced threshold is an artifact of our effective medium approximation or perhaps the process is catalytically assisted by dissociative adsorption of O_2 into more reactive atomic oxygen. A complex interplay ensues as the platinum layer grows, which not only changes the optical coupling and thus photothermal heating but also the in and out diffusion of the oxygen reactant and CO_x product.

As for our perspective on future work, we comment briefly. To purify thicker deposits, a multilayer deposit/purification sequence may be required, similar to what Mehendale et al.[41] demonstrated for a heated substrate process. In the limit, we suggest that an atomic layer deposition (ALD)-like process could be viable. While selective ALD deposits have been demonstrated using EBID deposits to locally catalyze reactions,[20] a truly direct-write ALD process is envisioned. Namely, the initial nanoscale half-reaction would be stimulated by the focused electron beam in the presence of the $MeCpPt^{IV}Me_3$ precursor to create thin PtC_x patterns. Subsequently, a synchronized laser pulse in the presence of oxygen would photothermally stimulate the carbon reduction half-reaction to create pure nanostructures.

ASSOCIATED CONTENT

Supporting Information

Effect of reactive gas in the laser annealing process, EDS spectra and quantitative analysis details, purification rate estimates, finite-difference numerical approximation method, thermal simulation details, simulated time−temperature profiles as a function of the pure platinum top-layer thickness, details about the effects of a pure platinum optical coupling underlayer, and more images of annealed deposits. This material is available free of charge via the Internet at http://pubs.acs.org.

AUTHOR INFORMATION

Corresponding Author

*E-mail: prack@utk.edu.

Notes

The authors declare no competing financial interest.

ACKNOWLEDGMENTS

The authors acknowledge that this research was conducted at the Center for Nanophase Materials Sciences, which is a DOE Office of Science User Facility. M.G.S. acknowledges support from the National Defense Science and Engineering Graduate Fellowship funded through the AFOSR. B.B.L. acknowledges support via the University of Tennessee Chancellor's Fellowship program. P.D.R. and J.D.F. acknowledge that their contributions (mentoring, design of experiments, modeling, manuscript preparation) was supported by the Center for Nanophase Materials Sciences which is a DOE Office of Science User Facility. Cheryl Hartfield at Omniprobe, Inc. (an Oxford Instruments Company) for assistance with the OmniGIS gas injection system. H.P. acknowledges support from Prof. Ferdinand Hofer, the Austrian Cooperative Research, and the Graz University of Technology in Austria.

REFERENCES

(1) Botman, A.; Mulders, J. J. L.; Hagen, C. W. Creating Pure Nanostructures from Electron-Beam-Induced Deposition using Purification Techniques: A Technology Perspective. *Nanotechnology* **2009**, *20*, 372001.

(2) Randolph, S. J.; Fowlkes, J. D.; Rack, P. D. Focused, Nanoscale Electron-Beam-Induced Deposition and Etching. *Crit. Rev. Solid State Mater. Sci.* **2006**, *31*, 55−89.

(3) Utke, I.; Moshkalev, S.; Russell, P. *Nanofabrication Using Focused Ion and Electron Beams: Principles and Applications*; Oxford University Press: Oxford, U.K., 2012.

(4) Utke, I.; Friedli, V.; Purrucker, M.; Michler, J. Resolution in Focused Electron- and Ion-Beam Induced Processing. *J. Vac. Sci. Technol. B* **2007**, *25*, 2219−2223.

(5) Smith, D. A.; Fowlkes, J. D.; Rack, P. D. Understanding the Kinetics and Nanoscale Morphology of Electron-Beam-Induced Deposition via a Three-Dimensional Monte Carlo Simulation: The Effects of the Precursor Molecule and the Deposited Material. *Small* **2008**, *4*, 1382−1389.

(6) Fowlkes, J. D.; Rack, P. D. Fundamental Electron−Precursor−Solid Interactions Derived from Time-Dependent Electron-Beam-Induced Deposition Simulations and Experiments. *ACS Nano* **2010**, *4*, 1619−1629.

(7) Rykaczewski, K.; White, W. B.; Fedorov, A. G. Analysis of Electron Beam Induced Deposition (EBID) of Residual Hydrocarbons in Electron Microscopy. *J. Appl. Phys.* **2007**, *101*, 054307.

(8) Toth, M.; Lobo, C. J.; Hartigan, G.; Knowles, W. R. Electron Flux Controlled Switching between Electron Beam Induced Etching and Deposition. *J. Appl. Phys.* **2007**, *101*, 054309.

(9) Utke, I.; Hoffmann, P.; Berger, R.; Scandella, L. High-Resolution Magnetic Co Supertips Grown by a Focused Electron Beam. *Appl. Phys. Lett.* **2002**, *80*, 4792−4794.
(10) Noh, J. H.; Nikiforov, M.; Kalinin, S. V.; Vertegel, A. A.; Rack, P. D. Nanofabrication of Insulated Scanning Probes for Electromechanical Imaging in Liquid Solutions. *Nanotechnology* **2010**, *21*, 365302.
(11) Serrano-Ramon, L.; Cordoba, R.; Rodriguez, L. A.; Magen, C.; Snoeck, E.; Gatel, C.; Serrano, I.; Ibarra, M. R.; De Teresa, J. M. Ultrasmall Functional Ferromagnetic Nanostructures Grown by Focused Electron-Beam-Induced Deposition. *ACS Nano* **2011**, *5*, 7781−7787.
(12) Gavagnin, M.; Wanzenboeck, H. D.; Belic, D.; Bertagnolli, E. Synthesis of Individually Tuned Nanomagnets for Nanomagnet Logic by Direct Write Focused Electron Beam Induced Deposition. *ACS Nano* **2013**, *7*, 777−784.
(13) Choo, H.; Kim, M. K.; Staffaroni, M.; Seok, T. J.; Bokor, J.; Cabrini, S.; Schuck, P. J.; Wu, M. C.; Yablonovitch, E. Nanofocusing in a Metal−Insulator−Metal Gap Plasmon Waveguide with a Three-Dimensional Linear Taper. *Nat. Photonics* **2012**, *6*, 837−843.
(14) Utke, I.; Jenke, M. G.; Roling, C.; Thiesen, P. H.; Iakovlev, V.; Sirbu, A.; Mereuta, A.; Caliman, A.; Kapon, E. Polarisation Stabilisation of Vertical Cavity Surface Emitting Lasers by Minimally Invasive Focused Electron Beam Triggered Chemistry. *Nanoscale* **2011**, *3*, 2718−2722.
(15) Koops, H. W. P.; Schossler, C.; Kaya, A.; Weber, M. Conductive Dots, Wires, and Supertips for Field Electron Emitters Produced by Electron-Beam Induced Deposition on Samples having Increased Temperature. *J. Vac. Sci. Technol. B* **1996**, *14*, 4105−4109.
(16) Yang, X.; Simpson, M. L.; Randolph, S. J.; Rack, P. D.; Baylor, L. R.; Cui, H.; Gardner, W. L. Integrated Tungsten Nanofiber Field Emission Cathodes Selectively Grown by Nanoscale Electron Beam-Induced Deposition. *Appl. Phys. Lett.* **2005**, *86*, 183106.
(17) Kolb, F.; Schmoltner, K.; Huth, M.; Hohenau, A.; Krenn, J. R.; Klug, A.; List, E. J. W.; Plank, H. Variable Tunneling Barriers in FEBID Based PtC Metal−Matrix Nanocomposites as a Transducing Element for Humidity Sensing. *Nanotechnology* **2013**, *24*, 305501.
(18) Schwalb, C. H.; Grimm, C.; Baranowski, M.; Sachser, R.; Porrati, F.; Reith, H.; Das, P.; Muller, J.; Volklein, F.; Kaya, A.; Huth, M. A Tunable Strain Sensor Using Nanogranular Metals. *Sensors* **2010**, *10*, 9847−9856.
(19) Guan, Y. F.; Fowlkes, J. D.; Retterer, S. T.; Simpson, M. L.; Rack, P. D. Nanoscale Lithography via Electron Beam Induced Deposition. *Nanotechnology* **2008**, *19*, 505302.
(20) Mackus, A. J. M.; Thissen, N. F. W.; Mulders, J. J. L.; Trompenaars, P. H. F.; Verheijen, M. A.; Bol, A. A.; Kessels, W. M. M. Direct-Write Atomic Layer Deposition of High-Quality Pt Nanostructures: Selective Growth Conditions and Seed Layer Requirements. *J. Phys. Chem. C* **2013**, *117*, 10788−10798.
(21) Rykaczewski, K.; Hildreth, O. J.; Kulkarni, D.; Henry, M. R.; Kim, S. K.; Wong, C. P.; Tsukruk, V. V.; Fedorov, A. G. Mask less and Resist-Free Rapid Prototyping of Three-Dimensional Structures Through Electron Beam Induced Deposition (EBID) of Carbon in Combination with Metal-Assisted Chemical Etching (MaCE) of Silicon. *ACS Appl. Mater. Interfaces* **2010**, *2*, 969−973.
(22) Seki, Y.; Furuta, Y.; Nishikawa, H.; Watanabe, T.; Nakata, T.; Satoh, T.; Ishii, Y.; Kamiya, T. Electroplating using High-Aspect-Ratio Microstructures Fabricated by Proton Beam Writing. *Microelectron. Eng.* **2009**, *86*, 945−948.
(23) Lassiter, M. G.; Liang, T.; Rack, P. D. Inhibiting Spontaneous Etching of Nanoscale Electron Beam Induced Etching Features: Solutions for Nanoscale Repair of Extreme Ultraviolet Lithography Masks. *J. Vac. Sci. Technol. B* **2008**, *26*, 963−967.
(24) Liang, T.; Frendberg, E.; Lieberman, B. Advanced Photolithographic Mask Repair using Electron Beams. *J. Vac. Sci. Technol. B* **2005**, *23*, 3101−3105.
(25) Noh, J. H.; Stanford, M. G.; Lewis, B. B.; Fowlkes, J. D.; Plank, H.; Rack, P. D. Nanoscale Electron Beam-Induced Deposition and Purification of Ruthenium for Extreme Ultraviolet Lithography Mask Repair. *Appl. Phys. A: Mater. Sci. Process.* **2014**, 1−9 DOI: 10.1007/s00339-014-8745-0.
(26) Bret, T.; Afra, B.; Becker, R.; Hofmann, T.; Edinger, K.; Liang, T.; Hoffmann, P. Gas Assisted Focused Electron Beam Induced Etching of Alumina. *J. Vac. Sci. Technol. B* **2009**, *27*, 2727−2731.
(27) Makise, K.; Mitsuishi, K.; Shimojo, M.; Shinozaki, B. Microstructural Analysis and Transport Properties of MoO and MoC Nanostructures Prepared by Focused Electron Beam-Induced Deposition. *Sci. Rep.* **2014**, *4*, 5740.
(28) Winhold, M.; Weirich, P. M.; Schwalb, C. H.; Huth, M. Superconductivity and Metallic Behavior in $Pb_xC_yO_\delta$ Structures Prepared by Focused Electron Beam Induced Deposition. *Appl. Phys. Lett.* **2014**, *105*, 162603.
(29) Brintlinger, T.; Fuhrer, M. S.; Melngailis, J.; Utke, I.; Bret, T.; Perentes, A.; Hoffmann, P.; Abourida, M.; Doppelt, P. Electrodes for Carbon Nanotube Devices by Focused Electron Beam Induced Deposition of Gold. *J. Vac. Sci. Technol. B* **2005**, *23*, 3174−3177.
(30) Botman, A.; Hesselberth, M.; Mulders, J. J. L. Improving the Conductivity of Platinum-Containing Nanostructures Created by Electron-Beam-Induced Deposition. *Microelectron. Eng.* **2008**, *85*, 1139−1142.
(31) Plank, H.; Gspan, C.; Dienstleder, M.; Kothleitner, G.; Hofer, F. The Influence of Beam Defocus on Volume Growth Rates for Electron Beam Induced Platinum Deposition. *Nanotechnology* **2008**, *19*, 485302.
(32) Gopal, V.; Radmilovic, V. R.; Daraio, C.; Jin, S.; Yang, P. D.; Stach, E. A. Rapid Prototyping of Site-Specific Nanocontacts by Electron and Ion Beam Assisted Direct-Write Nanolithography. *Nano Lett.* **2004**, *4*, 2059−2063.
(33) Botman, A.; Mulders, J. J. L.; Weemaes, R.; Mentink, S. Purification of Platinum and Gold Structures after Electron-Beam-Induced Deposition. *Nanotechnology* **2006**, *17*, 3779−3785.
(34) Langford, R. M.; Wang, T. X.; Ozkaya, D. Reducing the Resistivity of Electron and Ion Beam Assisted Deposited Pt. *Microelectron. Eng.* **2007**, *84*, 784−788.
(35) Stark, T. J.; Mayer, T. M.; Griffis, D. P.; Russell, P. E. Formation of Complex Features using Electron-Beam Direct-Write Decomposition of Palladium Acetate. *J. Vac. Sci. Technol. B* **1992**, *10*, 2685−2689.
(36) Klein, K. L.; Randolph, S. J.; Fowlkes, J. D.; Allard, L. F.; Meyer, H. M.; Simpson, M. L.; Rack, P. D. Single-Crystal Nanowires Grown via Electron-Beam-Induced Deposition. *Nanotechnology* **2008**, *19*, 345705.
(37) Fernandez-Pacheco, A.; De Teresa, J. M.; Cordoba, R.; Ibarra, M. R. Magnetotransport Properties of High-Quality Cobalt Nanowires Grown by Focused-Electron-Beam-Induced Deposition. *J. Phys. D: Appl. Phys.* **2009**, *42*, 055005.
(38) Tseng, A. A. *Nanofabrication: Fundamentals and Applications*; World Scientific: Singapore, 2008.
(39) Langford, R. M.; Ozkaya, D.; Sheridan, J.; Chater, R. Effects of Water Vapour on Electron and Ion Beam Deposited Platinum. *Microsc. Microanal.* **2004**, *10*, 1122−1123.
(40) Perentes, A.; Hoffmann, P. Focused Electron Beam Induced Deposition of Si-Based Materials from SiO_xC_y to Stoichiometric SiO_2: Chemical Compositions, Chemical-Etch Rates, and Deep Ultraviolet Optical Transmissions. *Chem. Vap. Deposition* **2007**, *13*, 176−184.
(41) Mehendale, S.; Mulders, J. J. L.; Trompenaars, P. H. F. A New Sequential EBID Process for the Creation of Pure Pt Structures from $MeCpPtMe_3$. *Nanotechnology* **2013**, *24*, 145303.
(42) Gopal, V.; Radmilovic, V. R.; Daraio, C.; Jin, S.; Yang, P. D.; Stach, E. A. Rapid Prototyping of Site-Specific Nanocontacts by Electron and Ion Beam Assisted Direct-Write Nanolithography. *Nano Lett.* **2004**, *4*, 2059−2063.
(43) Plank, H.; Noh, J. H.; Fowlkes, J. D.; Lester, K.; Lewis, B. B.; Rack, P. D. Electron-Beam-Assisted Oxygen Purification at Low Temperatures for Electron-Beam-Induced Pt Deposits: Towards Pure and High-Fidelity Nanostructures. *ACS Appl. Mater. Interfaces* **2014**, *6*, 1018−1024.

(44) Geier, B.; Gspan, C.; Winkler, R.; Schmied, R.; Fowlkes, J. D.; Fitzek, H.; Rauch, S.; Rattenberger, J.; Rack, P. D.; Plank, H. Rapid and Highly Compact Purification for Focused Electron Beam Induced Deposits: A Low Temperature Approach Using Electron Stimulated H_2O Reactions. *J. Phys. Chem. C* **2014**, *118*, 14009−14016.
(45) Takeguchi, M.; Shimojo, M.; Furuya, K. Post-Deposition Processes for Nanostructures Formed by Electron Beam Induced Deposition with $Pt(PF_3)_4$ Precursor. *Appl. Phys. A: Mater. Sci. Process.* **2008**, *93*, 439−442.
(46) Porrati, F.; Sachser, R.; Schwalb, C. H.; Frangakis, A. S.; Huth, M. Tuning the Electrical Conductivity of Pt-Containing Granular Metals by Postgrowth Electron Irradiation. *J. Appl. Phys.* **2011**, *109*, 063715.
(47) Roberts, N. A.; Fowlkes, J. D.; Magel, G. A.; Rack, P. D. Enhanced Material Purity and Resolution via Synchronized Laser Assisted Electron Beam Induced Deposition of Platinum. *Nanoscale* **2013**, *5*, 408−415.
(48) Roberts, N. A.; Gonzalez, C. M.; Fowlkes, J. D.; Rack, P. D. Enhanced By-product Desorption via Laser Assisted Electron Beam Induced Deposition of $W(CO)_6$ with Improved Conductivity and Resolution. *Nanotechnology* **2013**, *24*, 415301.
(49) Roberts, N. A.; Magel, G. A.; Hartfield, C. D.; Moore, T. M.; Fowlkes, J. D.; Rack, P. D. In situ Laser Processing in a Scanning Electron Microscope. *J. Vac. Sci. Technol. A* **2012**, *30*, 041404.
(50) Arnold, G.; Timilsina, R.; Fowlkes, J.; Orthacker, A.; Kothleitner, G.; Rack, P. D.; Plank, H. Fundamental Resolution Limits during Electron-Induced Direct-Write Synthesis. *ACS Appl. Mater. Interfaces* **2014**, *6*, 7380−7387.
(51) Plank, H.; Smith, D. A.; Haber, T.; Rack, P. D.; Hofer, F. Fundamental Proximity Effects in Focused Electron Beam Induced Deposition. *ACS Nano* **2012**, *6*, 286−294.
(52) Hopf, C.; Schluter, M.; Schwarz-Selinger, T.; von Toussaint, U.; Jacob, W. Chemical Sputtering of Carbon Films by Simultaneous Irradiation with Argon Ions and Molecular Oxygen. *New J. Phys.* **2008**, *10*, 093022.
(53) Hiratani, M.; Nabatame, T.; Matsui, Y.; Imagawa, K.; Kimura, S. Platinum Film Growth by Chemical Vapor Deposition based on Autocatalytic Oxidative Decomposition. *J. Electrochem. Soc.* **2001**, *148*, C524−C527.
(54) Campbell, C. T.; Ertl, G.; Kuipers, H.; Segner, J. A Molecular-Beam Study of the Adsorption and Desorption of Oxygen from a Pt(111) Surface. *Surf. Sci.* **1981**, *107*, 220−236.
(55) Matsushima, T.; Almy, D. B.; White, J. M. The Reactivity and Auger Chemical Shift of Oxygen Adsorbed on Platinum. *Surf. Sci.* **1977**, *67*, 89−108.
(56) Sachser, R.; Reith, H.; Huzel, D.; Winhold, M.; Huth, M. Catalytic Purification of Directly Written Nanostructured Pt Microelectrodes. *ACS Appl. Mater. Interfaces* **2014**, *6*, 15868−15874.